Effect of deformation of diamond anvil and sample in diamond anvil cell on the thermal conductivity measurement

Caihong Jia(贾彩红), Dawei Jiang(蒋大伟), Min Cao(曹敏), Tingting Ji(冀婷婷), and Chunxiao Gao(高春晓)
Citation: Chin. Phys. B, 2021, 30 (**12**): 124702. DOI: 10.1088/1674-1056/ac11d1
Journal homepage: http://cpb.iphy.ac.cn; http://iopscience.iop.org/cpb

What follows is a list of articles you may be interested in

Droplets breakup via a splitting microchannel

Wei Gao(高崴), Cheng Yu(于程), Feng Yao(姚峰)
Chin. Phys. B, 2020, 29 (**5**): 054702. DOI: 10.1088/1674-1056/ab7b4b

Electrohydrodynamic behaviors of droplet under a uniform direct current electric field

Zi-Long Deng(邓梓龙), Mei-Mei Sun(孙美美), Cheng Yu(于程)
Chin. Phys. B, 2020, 29 (**3**): 034703. DOI: 10.1088/1674-1056/ab6835

Multi-bubble motion behavior of uniform magnetic field based on phase field model

Chang-Sheng Zhu(朱昶胜), Zhen Hu(胡震), Kai-Ming Wang(王凯明)
Chin. Phys. B, 2020, 29 (**3**): 034702. DOI: 10.1088/1674-1056/ab6839

Phase field simulation of single bubble behavior under an electric field

Chang-Sheng Zhu(朱昶胜), Dan Han(韩丹), Sheng Xu(徐升)
Chin. Phys. B, 2018, 27 (**9**): 094704. DOI: 10.1088/1674-1056/27/9/094704

Three-dimensional multi-relaxation-time lattice Boltzmann front-tracking method for two-phase flow

Hai-Qiong Xie(谢海琼), Zhong Zeng(曾忠), Liang-Qi Zhang(张良奇)
Chin. Phys. B, 2016, 25 (**1**): 014702. DOI: 10.1088/1674-1056/25/1/014702

Effect of deformation of diamond anvil and sample in diamond anvil cell on the thermal conductivity measurement*

Caihong Jia(贾彩红), Dawei Jiang(蒋大伟), Min Cao(曹敏), Tingting Ji(冀婷婷), and Chunxiao Gao(高春晓)†

State Key Laboratory of Superhard Materials, Jilin University, Changchun 130000, *China*

(Received 29 April 2021; revised manuscript received 24 June 2021; accepted manuscript online 7 July 2021)

Studies show that the sample thickness is an important parameter in investigating the thermal transport properties of materials under high-temperature and high-pressure (HTHP) in the diamond anvil cell (DAC) device. However, it is an enormous challenge to measure the sample thickness accurately in the DAC under severe working conditions. In conventional methods, the influence of diamond anvil deformation on the measuring accuracy is ignored. For a high-temperature anvil, the mechanical state of the diamond anvil becomes complex and is different from that under the static condition. At high temperature, the deformation of anvil and sample would be aggravated. In the present study, the finite volume method is applied to simulate the heat transfer mechanism of stable heating DAC through coupling three radiative-conductive heat transfer mechanisms in a high-pressure environment. When the temperature field of the main components is known in DAC, the thermal stress field can be analyzed numerically by the finite element method. The obtained results show that the deformation of anvil will lead to the obvious radial gradient distribution of the sample thickness. If the top and bottom surfaces of the sample are approximated to be flat, it will be fatal to the study of the heat transport properties of the material. Therefore, we study the temperature distribution and thermal conductivity of the sample in the DAC by thermal-solid coupling method under high pressure and stable heating condition.

Keywords: diamond anvil cell, deformation, thermal conductivity, thermal-solid coupling method

PACS: 47.11.Fg, 07.35.+k, 51.20.+d, 92.60.hv **DOI:** 10.1088/1674-1056/ac11d1

1. Introduction

Investigating thermal transport properties of rocks and minerals under high-temperature and high-pressure (HTHP) conditions provides valuable clues to understand the physical and chemical properties of the mantle layer and dynamic processes of minerals inside the depth of the earth.[1–3] In this regard, the in-situ measurement technique of the diamond anvil cell (DAC) has been developed for investigating multiple physical properties of materials under extremely high pressures.[4–6] In order to measure thermal properties of material under HTHP conditions, a water-cooling DAC is designed in the present study. The designed apparatus is equipped with a vacuum device to realize a stable heat flow field in the DAC.[7] Thermal loads are caused by temperature inhomogeneity in the steady-state heating, and the influence of thermal loads on the structural reliability of DAC and measuring the sample thickness are the main challenges in the early stage of the experiment.[8–10] Yue *et al.* in our research group proposed the method of multi-thermocouple *in situ* temperature measurement combined with the numerical model to simulate the distribution of sample temperature field in DAC by heat conduction, and established a brand-new sample thermal conductivity measurement method.[7] However, the *in situ* thermal conductivity of samples studied by this method depends on the structural size of the main components of DAC. It is worth noting that at this moment, the stress state and deformation degree of diamond anvils (DAs) and sample under HTHP conditions are not clear. Meanwhile, the influence of anvil and sample deformation on the thermal conductivity measurement in the DAC has not been systematically simulated and analyzed.

When the DAC is applied to investigate electrical and heat transport properties of materials, it is necessary to know the exact thickness distribution of the sample under different temperature and pressure rather than an average or approximate thickness value to obtain the exact conductivity, thermal conductivity and Seebeck coefficients.[11] It is worth noting that the cupping deformation of DAs under high pressures makes the sample take on the shape of "convex lens". This is because an uneven face pressure of the sample results in a certain gradient distribution of the sample thickness.[12–14] Currently, two techniques are commonly applied to measure the sample thickness in the DAC. The first method is to measure the relative variation of distance between two marks on the side of DAs to reflect the *in situ* thickness of the compressed sample.[15] The main hypothesis in this method is that the diamond deformation under the HTHP condition is negligible. The second method is a new sample thickness calibration method proposed by Li *et al.*, where the influence of diamond anvils axial deformation on the sample thickness measurement is eliminated to the maximum extent.[11] However, the premise of these two methods is to assume that the surface of the sample is a plane, ignoring the influence of the DAs cupping deforma-

*Project supported by the National Key Research and Development Program of China (Grant No. 2018YFA0702700) and the National Natural Science Foundation of China (Grant Nos. 11674404 and 11774126).

†Corresponding author. E-mail: 2564335439@qq.com

tion on the accuracy of sample thickness measurement under extreme conditions.

When studying the heat transport properties of materials in water-cooling DAC, the type Ia DAs is fixed on the high-temperature seat, while the heat conduction and three-dimensional thermal radiation occur from the back surface of the top and bottom DAs to sample and spacer. For a high-temperature anvil, the mechanical state of the diamond anvil becomes complex and is different from that under the static condition. The thermal stress increases as the temperature increases, thereby intensifying the anvil deformation.[9] However, there are limitations in existing means of quantitative detection of anvil deformation under HTHP conditions. Accordingly, it is essential to carry out numerical simulations to quantitatively analyze DAs and sample deformation under HTHP condition and evaluate the influence on the measuring accuracy of sample thermal conductivity.

In the present study, it is intended to use a thermal-solid coupling method to analyze the thermal stress coupled field. In this regard, the finite volume method (FVM) is applied to analyze the radiation-conduction coupling heat transfer of the main components in DAC. Then, the obtained node temperature is applied as an external load to analyze the structural stress by the finite element method (FEM). The quantitative analysis shows that diamond anvil and sample deformation have great influence on the measuring accuracy of the sample thermal conductivity under extreme conditions. Therefore, the aim of present study is that the new numerical simulation method is proposed to measure the *in situ* thermal conductivity in diamond anvils cell under high pressure and stable heating condition. This article has presented the new thermal-solid coupling method to study the thermal transport conductivity of sample in the DAC. The method fully considers the influence of the deformation of the diamond anvil and the sample under HTHP on the accuracy of *in situ* thermal conductivity measurement, which provides a new idea for realizing the accurate measurement of the thermal transport properties of materials in extreme environments.

2. Mathematical model

For many thermal characteristics of materials, including Seebeck and thermal conductivity coefficients, a static temperature gradient must be considered along the axial (longitudinal) direction of the sample.[16,17] In order to prepare such an environment in the experiment, the steady-state method is used to realize the stable and constant heat flow environment of water-cooling DAC. In experiments, we often use type Ia diamond as anvil. Type Ia diamond contains aggregated impurity nitrogen atoms, and its nitrogen content is 1710 ppm. A high-temperature electric resistance furnace interacts with the type Ia DAs' back surfaces. In the present study, it is intended to investigate thermal behaviors of diamond anvils, sample and gasket (DASG). In this regard, Fig. 1 illustrates the established model. It should be indicated that the geometric structure of the DASG is consistent with the experiment. Since the diamond thermal conductivity is very high, the DAs' back surface is considered as a wall with a constant temperature. T_1 (T_2) denotes the back surface temperature of the top (bottom) DA, T_3 (T_4) denotes the temperature at the midpoint of the top (bottom) DA lateral edges.

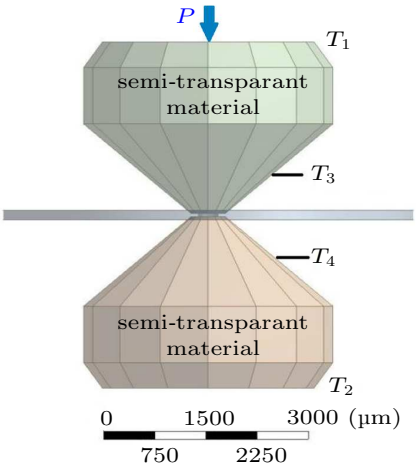

Fig. 1. Schematics of the diamond anvils, sample, and gasket in the simulation.

Diamond anvil is a semi-transparent material, and its radiation is involved in the heat transfer process.[18] Therefore, it is essential to consider the transmission and absorption of radiation inside the anvil. Accordingly, a spectrophotometer is used to characterize the thermal radiation characteristics of the type Ia diamond anvil. Through this way, affecting parameters, including the reflection spectrum R_λ, transmittance spectra T_λ, and absorption spectra A can be obtained (Fig. S1 of supporting information). The optical constant emissivity ε, absorption coefficient α and complex refractive index n can be calculated through the following expressions:

$$T_\lambda = \frac{(1-R_\lambda)^2 D}{1-R_\lambda^2 D^2}, \quad R_\lambda = \frac{(1-n)^2+k^2}{(1+n)^2+k^2},$$
$$D = \exp(-\alpha d), \qquad \alpha = 4\pi k v, \tag{1}$$

where d and v denote the diamond thickness and the heat ray frequency, respectively. Moreover, n and k are refractive indices. In the present study, the heat ray band is simplified into eight bands to describe the thermal radiation characteristics of type Ia DAs. Table 1 presents the corresponding thermal radiation characteristics.

In the experiment, the surrounding environment of the DAC is firstly vacuumed to 10^0 Pa to minimize the effects of natural convection before heating. Therefore, the influence of natural convection of vacuum air on the heat flow field of DAC can be ignored. In order to minimize the convective heat transfer between the solid calculation zone and the flow field around DAC, the calculation is carried out with assuming a

vacuum environment. Consequently, radiation is the dominant heat transfer mechanism in the vacuum environment and the heat loss of the outer wall of DAC is conducted by the surface radiation. Forgoing discussions demonstrate that the heat energy is transferred from the top and bottom anvil base to the sample through the conduction mechanism and three-dimensional radiation. Table 2 presents the properties of anvil, gasket and sample $MgSiO_3$.

Table 1. Thermal radiation characteristics of type Ia diamond.

Band (nm)	Emissivity	Absorption coefficient (cm^{-1})	Refractive index
200–470	0.28	1.83	1.95
470–580	0.15	0.56	1.96
580–2500	0.1	0.23	1.97
2500–3703	0.24	2.23	2.3
3703–6667	0.55	14.68	2.4
6667–9550	0.6	46.67	2.4
9550–10848	0.65	19.77	2.45
10848–50000	0.57	12.73	2.4

Table 2. Parameters of materials used in model calculations.

Property	Diamond	Sample	Spacer
Density (kg/m^3)	3520	function[23]	7000
Thermal conductivity (W/(m·K))	function[19]	function[24]	function[26]
Specific heat capacity (J/(kg·K))	function[20]	function[23]	460
Thermal expansion coefficient (K^{-1})	function[21]	function[25]	1.2×10^{-5}
Young's modulus (Pa)	function[22]	function[25]	2×10^{11}
Poisson's ratio	function[22]	function[25]	0.3

Function: Physical quantities vary with temperature and pressure.

3. Results and discussion

3.1. Thermal stress of diamond anvil in DAC under stable heating condition

The thermal load caused by the uneven temperature distribution of DAs in the stable heating DAC produces certain thermal stress. The stress distribution of DAC is calculated under static and high temperatures to study the influence of the temperature on the anvil stress. Figure S2 shows that the temperature field of DAs is simulated by FVM when the temperature T_1–T_2 is 400–420 K, 700–720 K, 1000–1020 K, and 1300–1320 K, respectively. Then, the simulation of the temperature field as the thermal load is applied to the structural stress analysis. It is worth noting that the stress boundary condition P is applied to the anvil base, and the stress distribution of DAC under HTHP is simulated by the FEM. In order to study the thermal stress of anvil at different HTHPs, the ratio of the thermal stress on the anvil face to the total stress is shown in Table 3.

As can be seen from Table 3, when the anvil is in a fixed temperature environment, the thermal stress ratio on the anvil surface would decrease with the increase of the pressure boundary condition P applied to the top anvil base. In comparison to the high pressure, the anvil face pressure under low pressure has a higher sensitivity to temperature. When the pressure boundary condition P is constant, the thermal stress ratio of the anvil face increases as the base temperature T_1/T_2 at the elastic deformation stage increases. Therefore, the contribution of the temperature to the pressure on the diamond anvil face cannot be ignored. For example, when the pressure boundary condition $P = 100$ MPa and the temperature T_1–T_2 of the top and bottom anvils' back surfaces increase from 400–420 K to 1300–1320 K, the stress on the anvil surface increases from 3.5 GPa to 4.2 GPa, and the thermal stress ratio on the anvil surface increases by 4.25% to 18.33%. The stress on the anvil surface would lead to the deformation of the anvil, and the significant increase of the thermal stress on the anvil surface would aggravate the deformation degree of the anvil. This means that when studying the thermal conductivity of materials under static heating in the DAC, attention should be paid to the deformation degree of anvil and sample thickness caused by thermal stress.

Table 3. The ratio of the thermal stress on the anvil face.

Boundary condition	Static	T_1–T_2: 400–420 K		T_1–T_2: 700–720 K		T_1–T_2: 1000–1020 K		T_1–T_2: 1300–1320 K	
P (MPa)	$P_{\text{anvil face}}$ (GPa)	$P_{\text{anvil face}}$ (GPa)	Ratio (%)	$P_{\text{anvil face}}$ (GPa)	Ratio (%)	$P_{\text{anvil face}}$ (GPa)	Ratio (%)	$P_{\text{anvil face}}$ (GPa)	Ratio (%)
100	3.4	3.5	4.25	3.8	11.27	4.0	15.27	4.2	18.33
330	11.6	11.8	1.30	12.1	3.76	12.2	4.78	12.5	7.14
500	17.9	18.1	1.13	18.3	2.05	18.3	2.26	18.4	2.58
770	27.4	27.6	0.73	27.8	1.34	27.9	1.76	30.0	1.97
1100	38.4	38.5	0.37	38.7	0.71	38.7	0.86	38.8	1.06

3.2. Effect of deformation diamond anvil and sample in DAC on the thermal conductivity measurement under stable heating condition

Figure 2(a) shows the deformation of the anvil when the average stress on the anvil face is 51.5 GPa. In order to observe the deformed shape more intuitively, the schematic diagram is based on the ratio of 1 : 30. Diamond would undergo "cup-shaped" deformation under high pressure, and the deformation of anvil would lead to the deformation of sample from initial cylindrical shape to "convex lens" shape.[12–14] It is observed that the shape variable of the anvil center region is greater than

the deformation of the edge region, which is consistent with the earlier experimental results.[8] Figures 2(b) and 2(c) illustrate the shape variables of the DAs under different pressures. The shape variable of DAs increases as the pressure increases. The intensification of the deformation of DAs results in an uneven surface pressure on the top and bottom surfaces of the sample, which will make the radial gradient distribution of the sample thickness more obvious.

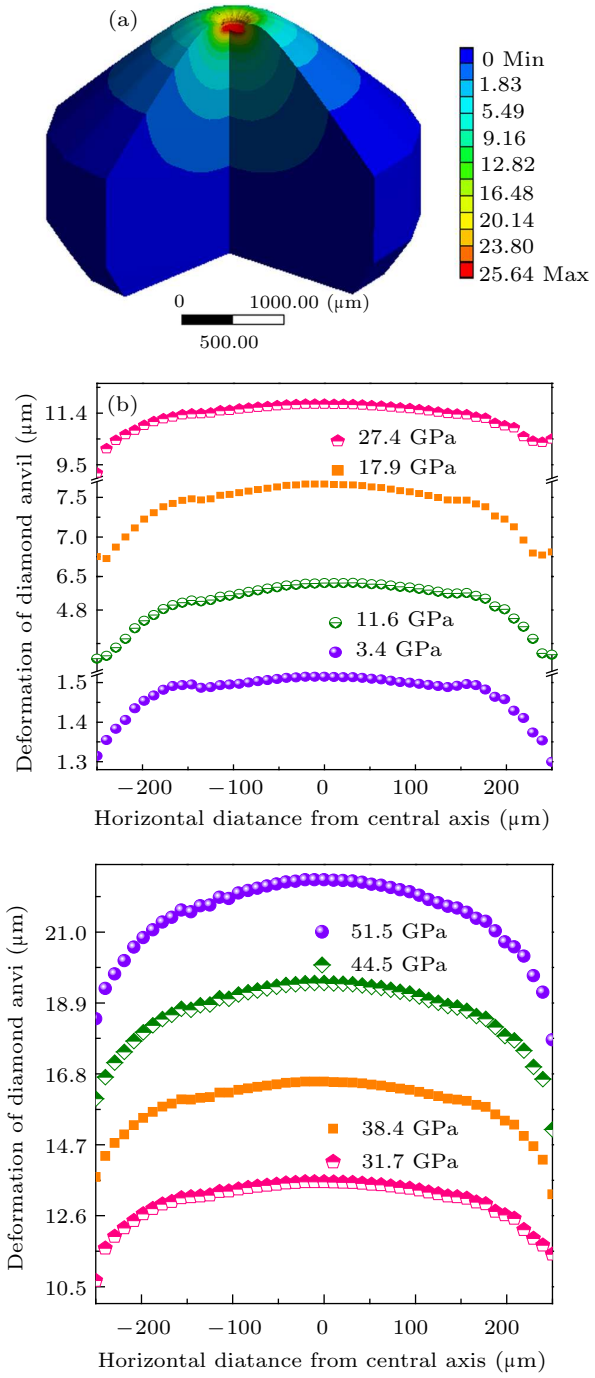

Fig. 2. (a) Deformation schematic of anvil under high pressure. (b) and (c) Deformation profiles of anvil under high pressure.

When the resistance furnace heats the anvil base directly, the heat conduction and the 3D radiation transmits from the anvils base to the sample. At this time, the whole anvil has a relatively high temperature distribution. High temperature causes obvious thermal stress on the anvil surface according the values in Table 3. Therefore, the influence of the temperature on anvil deformation under extreme conditions of HTHP is investigated. Figure 3 shows the shape variables of the anvil under high pressure when the temperatures T_1 and T_2 are controlled at 1300 K and 1320 K, respectively. Compared with Fig. 3, we find that the deformation of diamond anvil has changed obviously at high temperature. As can be found from Fig. 2, the gradient deformation of the anvil is relatively gentle near the center of the anvil surface, and mainly concentrated near the edge. Therefore, at room temperature, the pressure near the center of the anvil surface is generally considered to be a constant value, rather than a gradient distribution, that is, the top and bottom surfaces of the sample can be approximately considered to be planar. As can be seen from Fig. 3, under the action of thermal stress, the deformation near the center of the anvil face have obvious changes, and the gradient deformation degree in the center area of the anvil face is intensified. The same pressure boundary conditions are applied to the anvil base. The generated thermal stress increases the deformation degree of the anvil because of the thermal load.

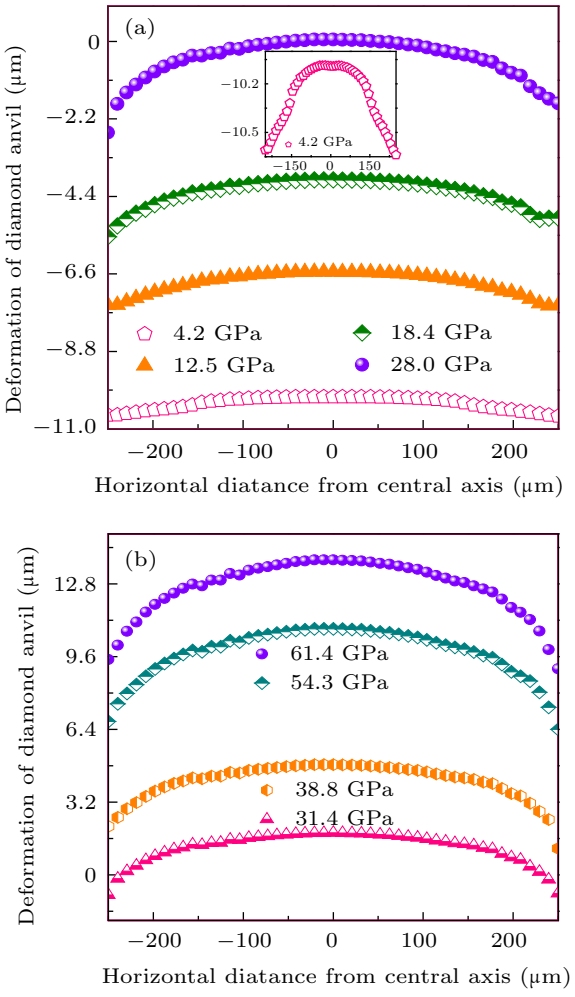

Fig. 3. Deformation profiles of the anvil under HTHP.

Because the deformation degree of anvil determines the deformation degree of sample thickness, the measurement error value of sample thickness in DAC would increase with the increase of temperature, so it is necessary to deeply analyze the influence of the anvil and sample deformation on the accuracy of thermal conductivity measurement under static heating in DAC.

In order to evaluate the influence of anvil deformation on sample thickness deformation in DAC, Tables 3 and 4 quantitatively show the cupping deformation of anvil under different pressure and temperature conditions, and the deformation ratio of sample thickness caused by this deformation. H_b is the distance between the center position of the top anvil surface and the center position of the bottom anvil surface, and H_a is the distance between the edge position of the top anvil surface and the edge position of the bottom anvil surface. H_{ab} is used to describe the cupping deformation degree of the diamond anvil. The calibration expression is

$$H_{ab} = H_b - H_a. \tag{2}$$

We compare the thickness deformation of the sample caused by the deformation of the anvil under different temperature conditions with the approximate plane of the sample surface, and obtain the deformation ratio of the sample thickness caused by the deformation of the diamond anvil in the following table. The calibration expression of sample deformation is

$$H_{s,max} = (H_b - H_a)/H_a, \quad H_{s,min} = (H_b - H_a)/H_b. \tag{3}$$

Tables 4 and 5 show the deformation degree value of the measured sample thickness, which presents an increasing trend with the increase of the anvil surface pressure and the temperature in DAC. When the stress boundary condition P is 100 MPa and the temperatures T_1–T_2 rise from static to 1300–1320 K, the pressure on the anvil face increases from 3.4 to 4.2 GPa, and the shape variable of the anvil increases from 0.41 to 1.05 μm, that is, the "concave" degree of the anvil surface increases. The most direct effect of anvil surface deformation is that the sample thickness presents gradient distribution. The value of deformation of sample thickness increases from 0.83%–0.84% to 2.07%–2.12%. Therefore, the higher the temperature is, the more significant the deformation degree in the measured sample thickness is. The sample thickness deformation caused by the anvil deformation cannot be ignored in DAC under high pressure and stable heating condition.

According to Fourier law $Q = \lambda \cdot S \cdot T/d$, the thermal flow Q flows through the sample with cross section S and thickness d, and the temperature difference in the thickness d direction is T, and the thickness deformation of the sample can lead to the corresponding error value in the measurement of the thermal conductivity of the sample. So big measurement error can be generated in sample traditional thickness measurements under static heating in the DAC.[10,11] Therefore, it is necessary to consider the experimental errors caused by anvil and sample deformation in order to realize the high-precision study of the sample thermal conductivity. Since numerical simulation can be used to quantitatively and systematically analyze the deformation degree of anvil and sample under static heating in the DAC at HTHP, the influence on *in situ* thermal conductivity measurement at HTHP is discussed. Then FVM and FEM can be used to establish a coupling field and the thermal-solid coupling can be used to study the structural deformation caused by thermal stress. The thermal-solid coupling calculation to deal with the structural deformation can avoid the influence of diamond anvil deformation and sample thickness gradient distribution on the *in situ* thermal conductivity measurement of materials in the DAC under high pressure and stable heating condition.

Table 4. Cupping deformation of anvils and deformation of sample thickness under high pressure.

Boundary condition	Anvil face pressure	Static			
P (MPa)	$P_{anvilface}$ (GPa)	H_a (μm)	H_b (μm)	H_{ab} (μm)	H_s (%)
100	3.4	48.88	49.29	0.41	0.83–0.84
330	11.6	46.41	47.85	1.44	3.01–3.10
500	17.9	44.66	46.78	2.11	4.52–4.73
770	27.4	41.47	45.4	3.92	8.64–9.46
900	31.7	39.91	44.52	4.61	10.35–11.55
1100	38.4	37.65	43.56	5.91	13.56–15.68

Table 5. Cupping deformation of anvils and deformation of sample thickness under HTHP.

Boundary condition	Anvil face pressure	T_1–T_2: 1300–1320 K			
P (MPa)	$P_{anvilface}$ (GPa)	H_a (μm)	H_b (μm)	H_{ab} (μm)	H_s (%)
100	4.2	49.81	50.86	1.05	2.07–2.12
330	12.5	47.21	49.29	2.07	4.2–4.39
500	18.4	45.09	48.12	3.03	6.3–6.73
770	28.0	42.07	46.39	4.31	9.3–10.25
900	31.7	40.41	45.6	5.19	11.38–12.84
1100	38.8	38.18	44.45	6.26	14.09–16.4

The thermal-solid coupling method we designed is a brand-new *in situ* thermal conductivity measurement method for samples. On the basis of knowing the initial geometric dimensions of the sample, the gasket and the anvil at normal pressure and room temperature, the thermal-solid coupling numerical model is used to obtain the true size and temperature distribution of the sample at HTHP, so as to obtain the accurate thermal conductivity of the sample. Therefore, the thermal-solid coupling method fully considers errors caused by deformation of DAs and sample, and effectively avoids the errors caused by traditional methods to measure the thickness of samples at different temperatures and pressures. In this scheme, ruby is placed in the center of the pressure chamber and four thermocouples are arranged, which are the top and bottom anvils' back surfaces and the midpoint of the DAs

lateral edges. The temperature T_1 and T_2 of the bases of the anvils' back are taken as the temperature boundary conditions and employed in the numerical simulation. At a certain temperature boundary, by changing the thermal conductivity of the sample and pressure boundary condition P, the input thermal conductivity considers the sample thermal conductivity at this pressure until the result of the simulated anvil surface pressure is the same as the measured pressure at the central anvil face by the ruby fluorescence method, and the simulating T_3 and T_4 are the same as the measured temperature at the midpoint of the DAs lateral edges by the thermocouples. That is to say, the real temperature distribution and accurate structural size of the anvil and the sample under HTHP are determined. The flow chart (Fig. S3) also explains the process of deducing the thermal conductivity of the sample under high pressure.

4. Conclusion

In conclusion, it is found that the conventional measurement method of the sample thickness in the DAC inevitably produces some errors for the thermal conductivity measurement under high pressure and stable heating condition. Moreover, the error increases as the temperature and pressure increase. The deformation of the diamond anvil and sample under HTHP is simulated by the numerical method. The results suggest that the deformation of anvil will lead to the obvious radial gradient distribution of the sample thickness. The deformation degree of the sample thickness can lead to the corresponding error value in the measurement of the thermal conductivity of the sample under extreme circumstances. Therefore, a new method is proposed to study the thermal transport properties of samples in the DAC by using the thermal-solid coupling to avoid the influence of anvil and sample thickness deformation on the thermal conductivity under extreme circumstances.

References

[1] Walker M, Stackhouse S, Wookey J, Forte A M, Brodholt J P and Dobson D P 2014 *Earth Planet. Sci. Lett.* **390** 175
[2] Lobanov S S, Holtgrewe N and Goncharov A F 2016 *Earth Planet. Sci. Lett.* **449** 20
[3] Koker N 2010 *Earth Planet. Sci. Lett.* **292** 392
[4] Ozawa H, Tateno S and Xie L 2018 *High Press. Res.* **38** 120
[5] Saha P, Mazumder A and Mukherjee G D 2020 *Geosci. Front.* **11** 1755
[6] Ai Q, Hu Z W, Wu L L, Sun F X and Xie M 2017 *Int. J. Heat Mass Transf.* **109** 1181
[7] Yue D H, Ji T T, Qin T. R, Wang J, Liu C L, Jiao H, Zhao L, Han Y H and Gao C X 2018 *Appl. Phys. Lett.* **112** 081901
[8] Hemley R J, Mao H K, Shen G Y, Badro J, Gillet P, Hanfland M and Hausermann D 1997 *Science* **276** 1242
[9] Jing M, Wu Q and Bi Y 2013 *Chin. J. High Press. Phys.* **27** 411
[10] Li M, Gao C X and Peng G 2007 *Rev. Sci. Instrum.* **78** 075106
[11] Gao C X, Han Y H and MA Y Z 2005 *Rev. Sci. Instrum.* **76** 083912
[12] Eremets M I 1996 *Measurement Science and Technology* **7** 0597
[13] Hemley R J, Mao H K and Shen G Y 1997 *Science* **276** 1242
[14] Mekel S, Hemley R J and MAO H K 1999 *Appl. Phys. Lett.* **74** 656
[15] Jing Q M, Bi Y and Wu Q 2007 *Rev. Sci. Instrum* **78** 073906
[16] Polvani D A, Fei Y, Meng J F and Badding J V 2000 *Rev. Sci. Instrum* **71** 3138
[17] Polvani D A, Meng J F, Hasegawa M and Badding J V 1999 *Rev. Sci. Instrum* **70** 3586
[18] Dore P L, Nucara A, Cannavò D, de Marzi G, Calvani P L, Marcelli A, Sussmann R S, Whitehead A J, Dodge C N, Krehan A J and Peter H J 1998 *Appl. Opt.* **37** 5731
[19] Olson J R, Pohl R O, Vandersande J W, Zoltan A, Anthony T R and Banholzer W F 1993 *Phys. Rev. B* **47** 14850
[20] Zain-ul-abdein M, Ijaz H and Saleem W 2017 *Materials* **10** 739
[21] Jacobsona P and Stoupinb S 2019 *Diam. Relat. Mater.* **97** 107469
[22] Valdez M N, Umemoto K and Wentzcovitch R M 2012 *Appl. Phys. Lett.* **101** 1
[23] Krupka K M, Hemingway B S, Robie R A and Kerrick D M 1985 *Am. Mineral.* **70** 261
[24] Ammann M W and Walker A M 2014 *Earth Planet. Sci. Lett.* **390** 175
[25] Qian W S, Wang W Z, Zou F and Wu Z Q 2018 *Geophys. Res. Lett.* **45** 665
[26] Yue D H, Gao Y, Zhao L, Yan Y L, Ji T T, Han Y H and Gao C X 2019 *Jpn. J. Appl. Phys.* **58** 040906